Biophysical Journal
Biophysical Letter

Asymmetric Phosphatidylethanolamine Distribution Controls Fusion Pore Lifetime and Probability

Alex J. B. Kreutzberger,[1] Volker Kiessling,[1] Binyong Liang,[1] Sung-Tae Yang,[1] J. David Castle,[2] and Lukas K. Tamm[1,*]

[1]Department of Molecular Physiology and Biological Physics and [2]Department of Cell Biology, Center for Cell and Membrane Physiology at the University of Virginia, Charlottesville, Virginia

ABSTRACT Little attention has been given to how the asymmetric lipid distribution of the plasma membrane might facilitate fusion pore formation during exocytosis. Phosphatidylethanolamine (PE), a cone-shaped phospholipid, is predominantly located in the inner leaflet of the plasma membrane and has been proposed to promote membrane deformation and stabilize fusion pores during exocytotic events. To explore this possibility, we modeled exocytosis using plasma membrane SNARE-containing planar-supported bilayers and purified neuroendocrine dense core vesicles (DCVs) as fusion partners, and we examined how different PE distributions between the two leaflets of the supported bilayers affected SNARE-mediated fusion. Using total internal reflection fluorescence microscopy, the fusion of single DCVs with the planar-supported bilayer was monitored by observing DCV-associated neuropeptide Y tagged with a fluorescent protein. The time-dependent line shape of the fluorescent signal enables detection of DCV docking, fusion-pore opening, and vesicle collapse into the planar membrane. Four different distributions of PE in the planar bilayer mimicking the plasma membrane were examined: exclusively in the leaflet facing the DCVs; exclusively in the opposite leaflet; equally distributed in both leaflets; and absent from both leaflets. With PE in the leaflet facing the DCVs, overall fusion was most efficient and the extended fusion pore lifetime (0.7 s) enabled notable detection of content release preceding vesicle collapse. All other PE distributions decreased fusion efficiency, altered pore lifetime, and reduced content release. With PE exclusively in the opposite leaflet, resolution of pore opening and content release was lost.

Membrane fusion is a necessary biological process for exocytosis, membrane trafficking, viral infection, and fertilization (1). Intracellular fusion as exemplified by exocytosis is mediated by a complex molecular machinery associated with the fusing membranes (2). At the core of this machinery are the soluble NSF attachment protein receptor (SNARE) proteins that alone are able to catalyze membrane fusion in vitro. According to current models, SNARE-mediated fusion occurs by formation of a stalk between the interacting membranes that elongates laterally and then opens to form a fusion pore that expands as the membranes fully fuse (3). Because highly curved membrane structures are necessary for the fusion pore and its preceding intermediates (4–7), lipid components that are favorable for generating curvature can enhance fusion (8). Phosphatidylethanolamine (PE) lipids are enriched in the inner leaflet of the plasma membrane (9,10); their conical shape confers a negative intrinsic curvature, which in turn could promote and stabilize pores during membrane fusion (11). It is therefore reasonable to hypothesize that the asymmetric distribution of PE between the two leaflets of the plasma membrane promotes fusion-pore formation in SNARE-mediated exocytosis and in models of this process. Simulations have predicted that PE could enhance the fusion rate when distributed on the outward facing leaflet of liposomes (12) or planar membranes (13). However, a comparative study of contrasting interleaflet PE distributions has not been performed due to the difficulty in preparing lipid bilayers with asymmetric lipid composition.

Recently, we reported SNARE-dependent fusion of purified dense core vesicles (DCVs; secretory vesicles from PC12 cells, an immortalized chromaffin cell line) with planar-supported bilayers containing the plasma membrane SNARE proteins syntaxin-1a and SNAP-25 (14). The supported bilayers were prepared by a two-step method that results in different lipid compositions of the first (substrate-proximal) and second (substrate-distal) leaflets (15–17). The DCVs contained neuropeptide Y (NPY) tagged with the fluorescent protein Ruby as content marker.

Submitted July 21, 2017, and accepted for publication September 13, 2017.

*Correspondence: lkt2e@virginia.edu

Alex J. B. Kreutzberger and Volker Kiessling contributed equally to this work.

Editor: Tobias Baumgart.

https://doi.org/10.1016/j.bpj.2017.09.014

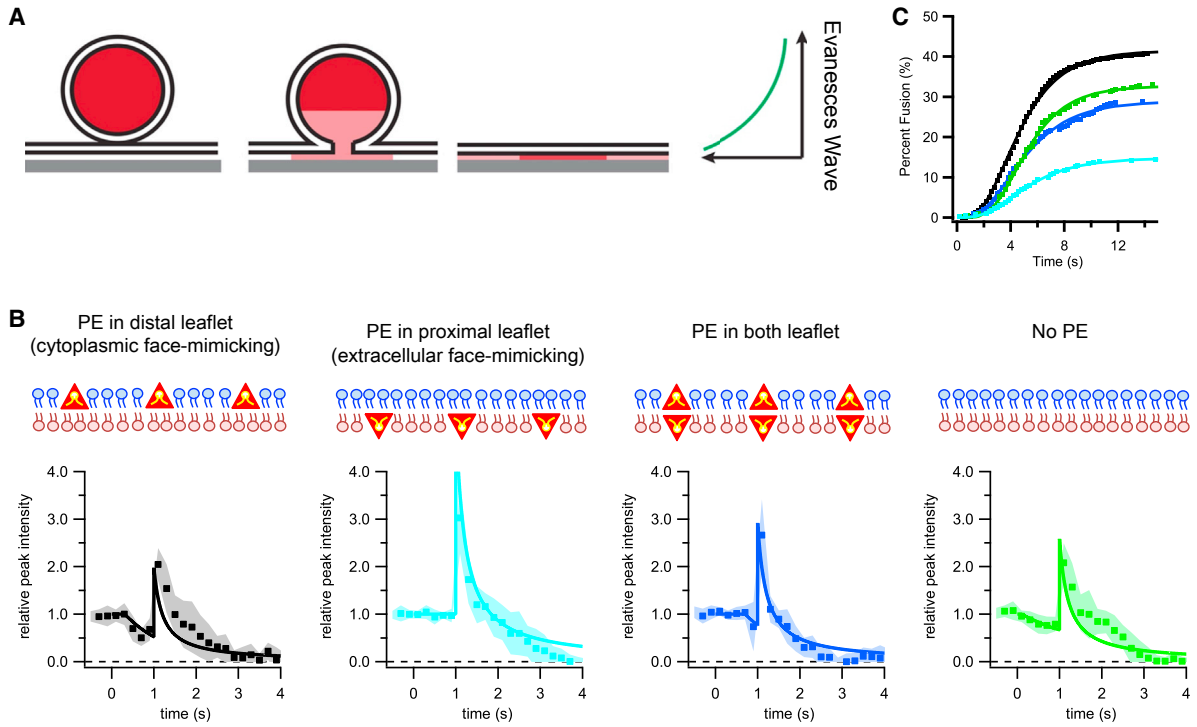

FIGURE 1 (*A*) Given here is a two-step model of DCV fusion event in a TIRF field. A DCV docks to a plasma membrane SNARE-containing planar-supported bilayer, where a fusion pore opens releasing the fluorescent NPY-Ruby from the DCV. The DCV then collapses into the supported bilayer, pulling NPY-Ruby forward in the TIRF field, which causes an increase in fluorescence as observed in the characteristic intensity traces of DCV fusion events. (*B*) Given here are characteristic fusion intensity traces for different distributions of PE in the supported bilayers. Dots are normalized intensities from 10 averaged fusion events, with SEs shown in shaded areas. Solid lines are fits of the two-step diffusion model shown in (*A*) with pore lifetimes of 0.7, 0, 0.3, and 1.5 s for PE in the distal, proximal, or both leaflets, or not present at all, respectively. A cartoon schematic of PE localization (*red triangles*) is shown above each figure, with blue and brown lipids representing the distal and proximal leaflets. (*C*) The kinetics of fusion are shown as cumulative distribution functions of the delay time between DCV docking and pore opening for PE in the distal leaflet (*black*), PE in the proximal leaflet (*cyan*), PE in both leaflets (*blue*), and no PE present (*green*).

Docking and fusion of single DCVs with the planar membrane was observed on a total internal reflection fluorescence (TIRF) microscope by following the fluorescence from NPY-Ruby. Upon docking, a sudden increase of fluorescence was detected as the DCV gets immobilized in the evanescent field. After a variable delay time, a first characteristic decay of fluorescent intensity occurs, followed by a sudden increase in fluorescence intensity, and ultimately a second characteristic decay of fluorescence was observed. This pattern is consistent with a two-step fusion process during which, first, a fusion pore opens, stays open whereas the DCV remains intact, and, in the second step, the DCV collapses into the planar membrane (Fig. 1 *A*). Fluorescent decays indicate diffusion of NPY-Ruby away from the fusion site and the intensity peak indicates a translocation of fluorescent content toward the substrate. A mathematical model that takes into account the characteristics of the evanescent electric field, the release rate through the fusion pore, and the lateral diffusion of NPY-Ruby within the cleft between the glass support and membrane, was able to reproduce the recorded fluorescence signal (14). In this model, the topology of the DCV was assumed not to change during the initial content release through the pore and NPY-mRuby in the DCV does not equilibrate, i.e., content is released first from within the proximity of the pore and only later from regions further away from the pore. A second requirement is that the lateral diffusion of NPY-mRuby away from the fusion site is faster during the first phase of release than after DCV collapse into the planar membrane. These conditions point to a relatively rigid luminal structure of the DCV protein content, which is strikingly similar to what was deduced from analyzing amperometric foot-signals measured during exocytotic events in chromaffin cells (18).

In this work we studied the effects of different PE distributions among the leaflets on fusion-pore stability, fusion efficiency, and fusion kinetics. We prepared plasma membrane SNARE-containing planar-supported bilayers under conditions with four different distributions of PE in the two leaflets: 1) 25 mol % in the distal leaflet facing the DCVs; 2) 25 mol % in the proximal (opposite) leaflet; 3) 25 mol % in both leaflets; and 4) no PE in either leaflet (Fig. 1 *B*). Condition 1 mimics the biological PE asymmetry of the plasma membrane and constitutes the same lipid distribution that was used in a recently published study (14).

The plasma membrane SNARE concentrations and orientations were the same under all four conditions (Fig. S2).

For each condition, we recorded at least 340 docking events of DCVs to plasma membrane SNARE-containing supported bilayers and evaluated their fusion efficiencies, fusion kinetics, and average line shapes, as described in detail in Kreutzberger et al. (14). The average line shapes measured under the different conditions were distinct in rate and length of the first decay as well as the following peak intensity (Fig. 1 *B*). The cumulative distribution functions of the time delays of the onset of fusion after docking were also different in the four cases (Fig. 1 *C*). The highest fusion efficiency, 41%, was achieved with PE in the distal, cytoplasmic face-mimicking leaflet of the target membrane. The fusion kinetics followed the same sigmoidal shape of previously reported single proteoliposome fusion events (Fig. 1 *C*; Table S1) (19). The fit of the fusion model to the average line shape of the fluorescence signal under condition 1 revealed a fusion pore that was open for 0.7 s and through which content was released with a characteristic rate of $(0.7\ s)^{-1}$ (Fig. 1 *B*; *black*). The diffusion coefficients for NPY-Ruby dispersion from the fusion site were 5 $\mu m^2/s$ during the initial release phase and 0.05 $\mu m^2/s$ after DCV collapse. These parameters are identical to the ones previously deduced under the same conditions (14), as recapitulated in the Supporting Material. For modeling the line shape of conditions 2–4, it was not necessary to change the two diffusion coefficients, showing that these parameters are independent of the fusion process.

For condition 2 (PE exclusively in the extracellular face-mimicking leaflet), fusion was strongly inhibited, with only ~15% of the docked DCVs undergoing fusion (Fig. 1 *C*, *cyan*). Moreover, the average line shape of these fusion events showed only a single phase, the collapse phase (Fig. 1 *B*, *cyan*). Within the time resolution of the measurement, 200 ms, no content release through a pore was detected and there was a compensatory increase in the fluorescence peak observed during DCV collapse. For condition 3 with symmetric PE distribution, the DCV fusion efficiency was 29%, about halfway between the two asymmetric conditions (Fig. 1 *C*, *blue*). Initial content release was observed and occurs at the same rate as under condition 1 $(0.7\ s)^{-1}$. However, the lifetime of the fusion pore was reduced to 0.3 s (Fig. 1 *B*, *blue*). For condition 4 (no PE; symmetric PC/cholesterol), the DCV fusion efficiency was 33% (similar to condition 3) (Fig. 1 *C*, *green*). In the average line shape, initial release of NPY-mRuby was clearly visible and the data were fitted with a characteristic release rate of $(1.5\ s)^{-1}$ and a fusion pore duration of 0.9 s (Fig. 1 *B*, *green*).

These results show that our hybrid system for reconstituting SNARE-mediated fusion in vitro using purified DCVs and supported membranes that contain only syntaxin-1a and SNAP-25 is able to reproduce the basic characteristics of single secretion events observed by amperometry of chromaffin cells (18). The fusion partners provide everything that is necessary to open a fusion pore and keep it open for almost 1 s. Our finding that the PE distribution is a key factor contributing to the presence of an initial release phase of NPY-Ruby through the stable fusion pore, has not been described before, to our knowledge. It experimentally confirms theories that invoke the importance of lipid shape in fusion intermediates. Indeed, under condition 1 with PE in the cytoplasmic-mimicking leaflet, about half of the fluorescent content is released before the DCV collapses into the planar target membrane. It is striking how well this asymmetric PE condition in our model membrane system not only promotes fusion with the highest efficiency but also reflects the electrophysiologically measured fusion events in cells (18). PE as a cone-shaped lipid most likely stabilizes the highly-curved local structure within the bilayer at the pore. Consistent with this view are our observations that no pore was observed when PE was present exclusively in the opposing leaflet and that a pore with shorter lifetime was observed with symmetrically distributed PE. Interestingly, when PE was absent on either side of the bilayer, release was observed over a longer time (0.9 s), but at a significantly slower rate. One interpretation of this result is that in the absence of PE, the pores transiently open and close instead of being stabilized by PE. This explanation is similar to that offered for single vesicle fusion as observed by TIRF microscopy by Stratton et al. (20).

In summary, we have shown how PE distribution contributes to the characteristic fluorescence profile that we observed in reconstituted SNARE-mediated fusion and how this distribution affects fusion probability, fusion pore stability, and the kinetics of DCV content release. In the future, our hybrid system should permit investigations of how other factors in the vesicle or plasma membrane influence the structure and stability of the exocytotic fusion pore.

SUPPORTING MATERIAL

Supporting Materials and Methods, Supporting Results, two figures, and one table are available at http://www.biophysj.org/biophysj/supplemental/S0006-3495(17)31026-3.

AUTHOR CONTRIBUTIONS

All authors designed the research, analyzed the data, and wrote or edited the article. A.J.B.K. and V.K. performed the research.

ACKNOWLEDGMENTS

We thank P. Kasson, D. Cafiso, and C. Stroupe for helpful discussions.

This work is supported by grant No. P01GM72694 from the National Institutes of Health (NIH).

SUPPORTING CITATIONS

References (21–34) appear in the Supporting Material.

REFERENCES

1. Martens, S., and H. T. McMahon. 2008. Mechanisms of membrane fusion: disparate players and common principles. *Nat. Rev. Mol. Cell Biol.* 9:543–556.
2. Südhof, T. C. 2013. Neurotransmitter release: the last millisecond in the life of a synaptic vesicle. *Neuron.* 80:675–690.
3. Hui, S. W., T. P. Stewart, …, P. L. Yeagle. 1981. Membrane fusion through point defects in bilayers. *Science.* 212:921–923.
4. Chizmadzhev, Y. A., F. S. Cohen, …, J. Zimmerberg. 1995. Membrane mechanics can account for fusion pore dilation in stages. *Biophys. J.* 69:2489–2500.
5. Chernomordik, L. V., and M. M. Kozlov. 2005. Membrane hemifusion: crossing a chasm in two leaps. *Cell.* 123:375–382.
6. Chernomordik, L. V., and M. M. Kozlov. 2008. Mechanics of membrane fusion. *Nat. Struct. Mol. Biol.* 15:675–683.
7. Jackson, M. B. 2009. Minimum membrane bending energies of fusion pores. *J. Membr. Biol.* 231:101–115.
8. Yeagle, P. L. 1989. Lipid regulation of cell membrane structure and function. *FASEB J.* 3:1833–1842.
9. Calderón, R. O., and G. H. DeVries. 1997. Lipid composition and phospholipid asymmetry of membranes from a Schwann cell line. *J. Neurosci. Res.* 49:372–380.
10. van Meer, G., D. R. Voelker, and G. W. Feigenson. 2008. Membrane lipids: where they are and how they behave. *Nat. Rev. Mol. Cell Biol.* 9:112–124.
11. Churchward, M. A., T. Rogasevskaia, …, J. R. Coorssen. 2008. Specific lipids supply critical negative spontaneous curvature—an essential component of native Ca^{2+}-triggered membrane fusion. *Biophys. J.* 94:3976–3986.
12. Kasson, P. M., and V. S. Pande. 2007. Control of membrane fusion mechanism by lipid composition: predictions from ensemble molecular dynamics. *PLOS Comput. Biol.* 3:e220.
13. Risselada, H. J. 2017. Membrane fusion stalks and lipid rafts: a love hate relationship. *Biophys. J.* 112:2475–2478.
14. Kreutzberger, A. J. B., V. Kiessling, …, L. K. Tamm. 2017. Reconstitution of calcium-mediated exocytosis of dense-core vesicles. *Sci. Adv.* 3:e1603208.
15. Kalb, E., S. Frey, and L. K. Tamm. 1992. Formation of supported planar bilayers by fusion of vesicles to supported phospholipid monolayers. *Biochim. Biophys. Acta.* 1103:307–316.
16. Crane, J. M., V. Kiessling, and L. K. Tamm. 2005. Measuring lipid asymmetry in planar supported bilayers by fluorescence interference contrast microscopy. *Langmuir.* 21:1377–1388.
17. Kiessling, V., B. Liang, and L. K. Tamm. 2015. Reconstituting SNARE-mediated membrane fusion at the single liposome level. *Methods Cell Biol.* 128:339–363.
18. Albillos, A., G. Dernick, …, M. Lindau. 1997. The exocytotic event in chromaffin cells revealed by patch amperometry. *Nature.* 389: 509–512.
19. Domanska, M. K., V. Kiessling, and L. K. Tamm. 2010. Docking and fast fusion of synaptobrevin vesicles depends on the lipid compositions of the vesicle and the acceptor SNARE complex-containing target membrane. *Biophys. J.* 99:2936–2946.
20. Stratton, B. S., J. M. Warner, …, B. O'Shaughnessy. 2016. Cholesterol increases the openness of SNARE-mediated flickering fusion pores. *Biophys. J.* 110:1538–1550.
21. Pabst, S., J. W. Hazzard, …, D. Fasshauer. 2000. Selective interaction of complexin with the neuronal SNARE complex. Determination of the binding regions. *J. Biol. Chem.* 275:19808–19818.
22. Liang, B., V. Kiessling, and L. K. Tamm. 2013. Prefusion structure of syntaxin-1A suggests pathway for folding into neuronal trans-SNARE complex fusion intermediate. *Proc. Natl. Acad. Sci. USA.* 110:19384–19389.
23. Dawidowski, D., and D. S. Cafiso. 2013. Allosteric control of syntaxin 1a by Munc18-1: characterization of the open and closed conformations of syntaxin. *Biophys. J.* 104:1585–1594.
24. Kreutzberger, A. J., B. Liang, …, L. K. Tamm. 2016. Assembly and comparison of plasma membrane SNARE acceptor complexes. *Biophys. J.* 110:2147–2150.
25. Domanska, M. K., V. Kiessling, …, L. K. Tamm. 2009. Single vesicle millisecond fusion kinetics reveals number of SNARE complexes optimal for fast SNARE-mediated membrane fusion. *J. Biol. Chem.* 284:32158–32166.
26. Wagner, M. L., and L. K. Tamm. 2001. Reconstituted syntaxin1a/SNAP25 interacts with negatively charged lipids as measured by lateral diffusion in planar supported bilayers. *Biophys. J.* 81:266–275.
27. van den Hoff, M. J., A. F. Moorman, and W. H. Lamers. 1992. Electroporation in 'intracellular' buffer increases cell survival. *Nucleic Acids Res.* 20:2902.
28. Kiessling, V., J. M. Crane, and L. K. Tamm. 2006. Transbilayer effects of raft-like lipid domains in asymmetric planar bilayers measured by single molecule tracking. *Biophys. J.* 91:3313–3326.
29. Zhang, Z., Y. Wu, …, M. B. Jackson. 2011. Release mode of large and small dense-core vesicles specified by different synaptotagmin isoforms in PC12 cells. *Mol. Biol. Cell.* 22:2324–2336.
30. Kiessling, V., and L. K. Tamm. 2003. Measuring distances in supported bilayers by fluorescence interference-contrast microscopy: polymer supports and SNARE proteins. *Biophys. J.* 84:408–418.
31. Zareh, S. K., M. C. DeSantis, …, Y. M. Wang. 2012. Single-image diffusion coefficient measurements of proteins in free solution. *Biophys. J.* 102:1685–1691.
32. Fromherz, P., V. Kiessling, …, G. Zeck. 1999. Membrane transistor with giant lipid vesicle touching a silicon chip. *Appl. Phys. A.* 69:571–576.
33. Kiessling, V., B. Müller, and P. Fromherz. 2000. Extracellular resistance in cell adhesion measured with a transistor probe. *Langmuir.* 16:3516–3521.
34. Press, W. H., B. P. Flannery, …, W. T. Vetterling. 1986. Numerical Recipes: The Art of Scientific Computing.. Cambridge University Press, Cambridge, United Kingdom.

Biophysical Journal, Volume *113*

Supplemental Information

Asymmetric Phosphatidylethanolamine Distribution Controls Fusion Pore Lifetime and Probability

Alex J.B. Kreutzberger, Volker Kiessling, Binyong Liang, Sung-Tae Yang, J. David Castle, and Lukas K. Tamm

Materials and Methods

Materials

The following materials were purchased and used without further purification: porcine brain L-α-phosphatidylcholine (bPC), porcine brain L-α-phosphatidylethanolamine (bPE), porcine brain L-α-phosphatidylserine (bPS), bovine liver L-α-phosphatidylinositol (PI), phosphatidylinositol 4,5-bisphosphate ($PI4,5P_2$), 1,2-dioleoyl-*sn*-glycero-3-phosphoethanolamine-N-(lissamine rhodamine B sulfonyl) (Rh-DOPE), and 1,2-dioleoyl-*sn*-glycero-3-phosphoethanolamine-N-(7-nitro-2-1,3-benzoxadiazol-4-yl) (NBD-DOPE) were from Avanti Polar Lipids (Alabaster, Al). 1,2-dimyristoyl-*sn*-glycero-3--phosphoethanolamine-PEG3400-triethoxysilane (DPS) was from Shearwater Polymers (Huntsville, AL). Cholesterol, sodium cholate, 2,2',2'',2'''-(ethane-1,2-diyldinitrilo)tetraacetic acid (EDTA), calcium (Ca^{2+}), OptiPrep density gradient medium, sucrose, 3-(N-morpholino)propanesulfonic acid (MOPS), L-glutamic acid potassium salt monohydrate, potassium acetate, and glycerol were from Sigma (St. Louis, MO); 3-[(3-cholamidopropyl)dimethylammonio]-1-propanesulfonate (CHAPS) and dodecylphosphocholine (DPC) were from Anatrace (Maumee, OH); 2-[4-(2-hydroxyethyl)piperazin-1-yl]ethanesulfonic acid (HEPES) was from Research Products International (Mount Prospect, IL); chloroform, ethanol, Contrad detergent, all inorganic acids, bases, and hydrogen peroxide were from Fisher Scientific (Fair Lawn, NJ). Water was purified first with deionizing and organic-free 3 filters (Virginia Water Systems, Richmond, VA) and then with a NANOpure system from Barnstead (Dubuque, IA) to achieve a resistivity of 18.2 MΩ/cm.

Protein purification

Syntaxin-1a (constructs of residues 183-288) and wild-type SNAP-25A from *Rattus norvegicus* were expressed in *Escherichia coli* strain BL21(DE3) cells under the control of the T7 promoter in the pET28a expression vector and purified as described previously (21-24). Briefly, all proteins were purified using the Ni-NTA affinity chromatography. After the removal of N-terminal His-tags by thrombin cleavage, proteins were further purified by subsequent ion-exchange or size-exclusion chromatography when necessary. Wild-type SNAP-25 was quadruply dodecylated through disulfide bonding of dodecyl methanethiosulfonate (Toronto Research Company, Toronto, Ontario) to its four native cysteines (24). All SNAP-25 used in this work

refers to this lipid-anchored form of SNAP-25A. Purities of all proteins were verified by SDS-PAGE.

Reconstitution of SNAREs into proteoliposomes

Proteoliposomes with lipid composition of 25:25:15:30:4:1 bPC:bPE:bPS:Chol:PI: PI4,5P_2 for PE in the distal leaflet or 50:15:30:4:1 bPC:bPS:Chol:PI: PI4,5P_2 for no PE in the proximal leaflet were prepared. All t-SNARE proteins were reconstituted using sodium cholate as previously described (25, 26). The desired lipids were mixed and organic solvents were evaporated under a stream of N_2 gas followed by vacuum desiccation for at least 1 hour. The dried lipid films were dissolved in 181 μL of 25 mM sodium cholate in buffer (20 mM HEPES, 150 mM KCl, pH 7.4) followed by the addition of an appropriate volume of syntaxin-1a and SNAP-25A in their respective detergents to reach a final lipid to protein ratio of 3000 for each protein. After 1 hour of equilibration at room temperature, the mixture was diluted below the critical micellar concentration by adding more buffer to the desired final volume of 550 μL. The sample was then dialyzed overnight against 1 L of buffer with 1 buffer change after ~4 hours.

Preparation of planar supported bilayers containing SNARE acceptor complexes

Planar supported bilayers with reconstituted plasma membrane SNAREs were prepared by the Langmuir-Blodgett/vesicle fusion technique as described in previous studies (15, 26). Quartz slides were cleaned by dipping in 3:1 sulfuric acid:hydrogen peroxide for 15 minutes using a Teflon holder. Slides were then rinsed thoroughly in water. The first leaflet of the bilayer was prepared by Langumir-Blodgett transfer directly onto the quartz slide using a Nima 611 Langmuir-Blodgett trough (Nima, Conventry, UK) by applying the lipid mixture of 70:30:3 bPC:Chol:DPS for no PE in the proximal leaflet or 45:25:30:3 bPC:bPE:Chol:DPS for PE in the proximal leaflet from a chloroform solution. After allowing the solvent to evaporate for 10 minutes, the monolayer was compressed at a rate of 10 cm^2/minute to reach a surface pressure of 31 mN/m. After equilibration for 5 to 10 minutes, a clean quartz slide was rapidly (200 mm/minute) dipped into the trough and slowly (5 mm/minute) withdrawn, while a computer maintained a constant surface pressure and monitored the transfer of lipids with head groups down onto the hydrophilic substrate. Proteoliposomes reconstituted with 1:1 syntaxin-1a (residues 183-288):SNAP-25 at a lipid/protein ratio of 3000 were incubated with the Langmuir-

Blodgett monolayer to form the outer leaflet of the planar supported bilayer. A concentration of 77 μM total lipid in 1.3 mL total volume was used and the lipid composition of the outer leaflet was as indicated in the text. After incubation of the proteoliposomes for 2 hours the excess proteoliposomes were removed by perfusion with 10 mL of buffer (120 mM potassium glutamate, 20 mM potassium acetate, 20 mM HEPES, pH 7.4). The reconstitution efficiencies and orientation of syntaxin-1a under the four membrane preparations were almost identical. This was measured using site directed fluorescence labeling and Co2+ quenching as previously described (22) and illustrated in Supplemental Figure S2.

Cell culture

As previously described (14), pheochromocytoma cells (PC12) were cultured on 10 cm plastic cell culture plates at 37^{o}C in 10% CO_2 in Dulbecco's Modified Eagle Medium (DMEM) High Glucose 1 X Gibco supplemented with 10% horse serum (Cellgro), 10% calf serum (Fe^{+}) (Hyclone), and 1% penicillin/streptomycin mix. Medium was changed every 2-3 days and cells were passed after reaching 90% confluency by incubating 5 min in HBSS and replating in fresh medium. Cells were transfected with a plasmid carrying NPY-mRuby (14) by electroporation using an Electro Square Porator ECM 830 (BTX). After harvesting and sedimentation, cells were suspended in a small volume of sterile cytomix electroporation buffer (27) (120 mM KCl, 10 mM KH_2PO_4, 0.15 mM $CaCl_2$, 2 mM EGTA, 25 mM HEPES-KOH, 5 mM $MgCl_2$, 2 mM ATP, and 5 mM glutathione, pH 7.6) and then counted and diluted to ~14 x 10^6 cells/mL. 700 μL of cell suspension (~10x10^6 cells) and 30 μg of DNA were placed in an electroporator cuvette with 4 mm gap and two 255V, 8 ms electroporation pulses were applied. Cells were then transferred to a 10 cm cell culture dish with 10 mL of normal growth medium. NPY-mRuby transfected cells were cultured under normal conditions for 3 days after transfection and then used for fractionation.

DCV purification

As previously described (14), DCVs were purified using iso-osmotic media as follows. PC12 cells (15-30 10-cm plates depending on experiments) were scraped into PBS, pelleted by centrifugation, resuspended, and washed once in homogenization medium (0.26 M sucrose, 5 mM MOPS, and 0.2 mM EDTA). Following resuspension in 3 mL homogenization medium

containing protease inhibitor (Roche Diagnostics), the cells were cracked open using a ball bearing homogenizer with a 0.2507-inch bore and 0.2496-inch diameter ball. The homogenate was then spun at 4000 rpm (1000 x g) for 10 min at 4^{o}C in a fixed-angle microcentrifuge to pellet nuclei and larger debris. The postnuclear supernatant (PNS) was collected and spun at 11,000 rpm (8000 x g), 15 min at 4^{o}C to pellet mitochondria. The postmitochondrial supernatant (PMS) was then collected, adjusted to 5 mM EDTA, and incubated for 10 min on ice. A working solution of 50% Optiprep (iodixanol) (5 vol 60% Optiprep: 1 vol 0.26 M sucrose, 30 mM MOPS, 1 mM EDTA) and homogenization medium were mixed to prepare solutions for discontinuous gradients in Beckman SW55 tubes: 0.5 mL of 30% iodixanol on the bottom and 3.8 mL of 14.5% iodixanol, above which 1.2 ml EDTA-adjusted PMS was layered. Samples were spun at 45,000 rpm (190,000 x g_{av}) for 5 hours. A clear white band at the interface between the 30% and 14.5% iodixanol regions was collected as the DCV sample. The DCV sample was then extensively dialyzed in a cassette with 10,000 kD molecular weight cutoff (24-48 h, 3 x 5L) into the fusion assay buffer (120 mM potassium glutamate, 20 mM potassium acetate, 20 mM HEPES, pH 7.4).

Total internal reflection fluorescence (TIRF) microscopy

Experiments examining single-vesicle docking and fusion events were performed on a Zeiss Axiovert 35 fluorescence microscope (Carl Zeiss, Thornwood, NY), equipped with a 63x water immersion objective (Zeiss; N.A. = 0.95) and a prism-based TIRF illumination. The light source was an OBIS 532 LS laser from Coherent Inc. (Santa Clara, CA). Fluorescence was observed through a 610 nm band pass filter (D610/60; Chroma, Battleboro, VT) by an electron multiplying CCD (DU-860E; Andor Technologies). The prism-quartz interface was lubricated with glycerol to allow easy translocation of the sample cell on the microscope stage. The beam was totally internally reflected at an angle of 72^{o} from the surface normal, resulting in an evanescent wave that decays exponentially with a characteristic penetration depth of ~100 nm. An elliptical area of 250 x 65 μm was illuminated. The laser intensity, shutter, and camera were controlled by a homemade program written in LabVIEW (National Instruments, Austin, TX).

Single DCV fusion assay

Acceptor t-SNARE protein-containing planar supported bilayers were washed with fusion buffer containing EDTA. They were then perfused with DCVs (50-100 μL depending on preparation) diluted into 2 mL of fusion buffer (120 mM potassium glutamate, 20 mM potassium acetate, 20 mM HEPES, 100 μM EDTA, pH 7.4). After injection of the DCV sample, the microscope was focused within no more than 30 seconds and then 5000 images were taken with 200-ms exposure times and spooled directly to the hard drive. One spooling set was taken for each bilayer.

Single-vesicle fusion data were analyzed using a homemade program written in LabView (National Instruments). Stacks of images were filtered by a moving average filter. The maximum intensity for each pixel over the whole stack was projected on a single image. Vesicles were located in this image by a single-particle detection algorithm described in Kiessling et al. (28). The peak (central pixel) and mean fluorescence intensities of a 5 pixel x 5 pixel area around each identified center of mass were plotted as a function of time for all particles in the image series. The exact time points of docking and fusion were determined from the central pixel similar to pervious work (25). Cumulative distributions were determined from the time of docking to the time of fusion for individual fusion events and the fusion efficiency was determined from the number of vesicles that underwent fusion compared with the total number of vesicles that docked within 15 seconds of DCV docking.

Supplemental Results

Two-step Mathematical Fusion/Diffusion Model to Simulate Single DCV Fluorescence Intensity Traces

The fluorescence signal originating from the DCVs during fusion follows a characteristic line shape (Figure 1, Supplemental Figure 1). In the following paragraphs we reiterate a previously published description of a simple 2-step fusion/diffusion model that reproduces the basic features of the signal (14).

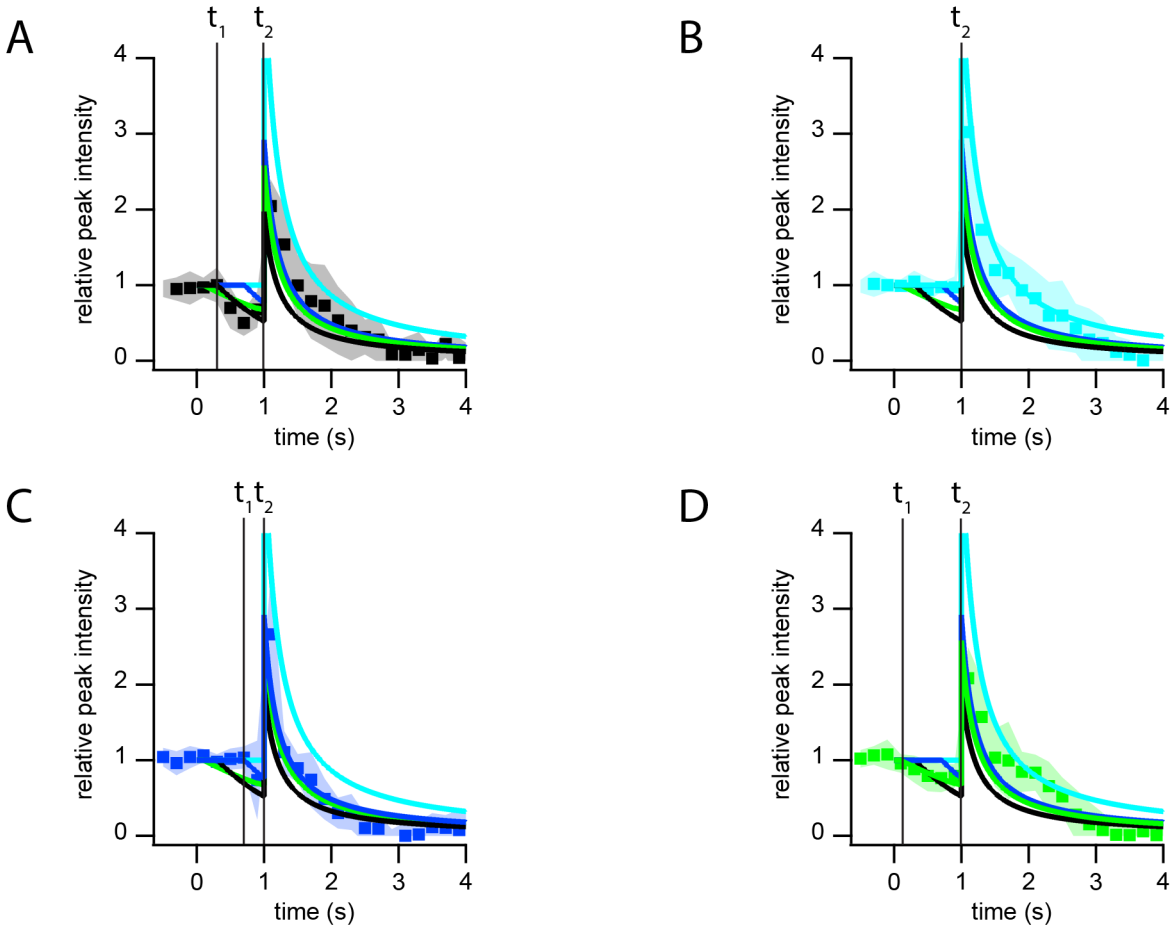

Supplemental Figure S1: *Averaged peak fluorescence during single DCV fusion events to supported membranes with four different trans-bilayer PE distributions: A) PE in the distal leaflet (black). B) PE in the proximal leaflet (cyan). C) PE in both leaflets (blue). D) without PE (green). The data are normalized to the intensity during docking, i.e. before fusion starts. For comparison, we combined the best simulated curves of all conditions with each data set.*

At each time the fluorescence originating from the fluorophore mRuby is determined by the sum of the fluorophore fraction located in the lumen of the DCV at a concentration C_{DCV} and the fraction in the small cleft between supported membrane and substrate at concentration C_{CLEFT}:

$$I = I_{DCV}(C_{DCV}(t, x, y), \lambda) + I_{CLEFT}(C_{CLEFT}(t, x, y, D), \lambda) \quad (1)$$

The model starts with a DCV of diameter d_{DCV}= 200 nm (28) docked at the supported lipid bilayer at distance z_0=8 nm (30) from the substrate and at x,y = 0. For the observed intensities, we take into account the 2D point spread function at λ = 600 nm and the decay of the evanescent wave with a characteristic penetration depth of d_p = 100 nm:

$$I_0 = I_{DCV}(t < t_1) = PSF(\lambda) * \int_{z_0}^{z_0 + d_{DCV}} C_{DCV}(x, y, z)\, e^{\frac{-z}{d_p}}\, dz \quad (2)$$

At time t_1 a fusion pore opens and content from the DCV gets released through the supported membrane into the cleft with a characteristic rate k_r at x,y = 0:

$$r(t - t_1) = e^{-\frac{(t - t_1)}{k_r}} \quad (3)$$

It is important to note that the characteristic rate might be limited by the release from the DCV's luminal structure or the diffusion through the fusion pore. Fluorescent content in the cleft is located at an average distance z_{CLEFT} = 2 nm (29) and spreads laterally in the x,y plane by free diffusion characterized by a diffusion coefficient D_1.

$$dC_{CLEFT}(t_1 < t < t_2) = [dr + D_1 \Delta C_{CLEFT}]dt \quad (4)$$

$$I_{CLEFT}(t_1 < t < t_2) = PSF(\lambda) * C_{CLEFT}(x, y, z, t)\, e^{\frac{-z_{CLEFT}}{d_p}} \quad (5)$$

During the life time of the fusion pore ($t_1 < t < t_2$) the shape of the DCV stays intact and content gets released from membrane proximal areas first (Figure 1A). A simpler model in which the distribution of content inside the DCV stays homogenous did not fit the data sufficiently. The fluorescence intensity originating from the DCV during this phase becomes:

$$I_{DCV}(t_1 < t < t_2) = PSF(\lambda) * \int_{z_1(t)}^{z_0 + d_{DCV}} C_{DCV}(x, y, z)\, e^{\frac{-z}{d_p}}\, dz \quad (6)$$

with $z_1(t)$ changing over time as more and more content gets released.

At time t_2 the DCV with its remaining content in the distal region from the supported membrane collapses into the SLB and diffuses together with the already released content laterally within the

cleft with an effective diffusion coefficient D_2. It is possible that parts of the luminal matrix in which the NPY is embedded (18) is still intact and that the observed fluorescent decay is limited by a release step from this structure. The effective diffusion coefficient therefore describes both, the release from the matrix and the actual lateral diffusion away from the fusion site.

$$C_{CLEFT}(t = t_2) = C_{CLEFT}(x, y, z, t_2) + C_{DCV}(x, y, z, t_2) \quad (7)$$

$$dC_{CLEFT}(t > t_2) = D_2 \Delta C_{CLEFT} dt \quad (8)$$

At this time (t_2) we assume the remaining content to collapse into a plane corresponding to the surface area of the original DCV instantaneously. The total observable intensity which now originates only from the cleft becomes:

$$I_{CLEFT}(t > t_2) = PSF(\lambda) * C_{CLEFT}(x, y, z, t)\, e^{\frac{-z_{CLEFT}}{d_p}} \quad (9)$$

We simulated the fluorescence intensity of the central pixel centered on a DCV using the above parameters and adjusting the length of the time period t_2-t_1, the release rate k_r. The diffusion coefficients D_1 and D_2 were left unchanged from our previous results (14). Figure 1B shows the best simulated curves together with data for the four lipid conditions used. In the Supplemental Figure S1 we show each data set combined with the best fit simulation for all membrane conditions to illustrate the detected differences in fusion pore life times and release rates. In the shown simulations, the released DCV content diffuses away from the fusion site with a rate of D_1 = 5 $\mu m^2/s$ during pore opening and with a diffusion coefficient of D_2 =0.05 $\mu m^2/s$ after collapse of the vesicle into the supported membrane. Both diffusion coefficients are significantly smaller than the reported diffusion coefficient for green fluorescent protein in solution ($D \approx 80\ \mu m^2/s$, (31)) indicating that the content indeed diffuses in the cleft between the supported membrane and substrate where the molecular mobility is known to be impaired (32,33). The slower diffusion observed after the collapse of the DCV might be due to the high density of (protein-) material at the fusion site and a possible release step of NPY.

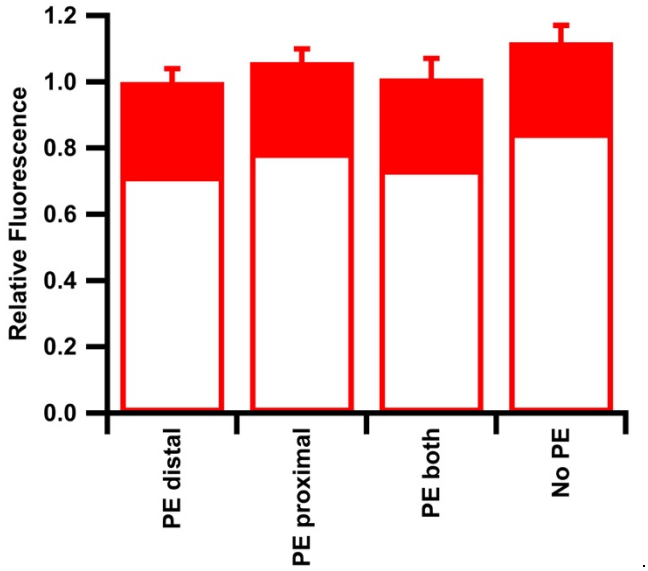

Supplemental Figure S2: *Relative fluorescence intensity of Alexa546-syntaxin-14C co-reconstituted with SNAP-25A into different types of planar supported bilayers. The protein was labeled and fluorescence was measured as described in Liang et al. 2013 (22). All intensities were normalized to condition 1 and the error bars represent the standard deviation of 8 images. The open bar area represents the amount of fluorescence that was quenched after 500 mM* Co^{2+} *was added to the sample indicating that 70-75% of all Alexa546-syntaxin-14C was oriented with its N-terminus facing away from the substrate.*

Condition	Proximal Leaflet	Distal Leaflet	Number of Experiments	Percent Fusion	Number of Docking	Number of Fusion	k (s^{-1})	m
PE Distal	70:30 bPC:Chol	25:25:15:30:4:1 bPC:bPE:bPS:Chol:PI:PIP2	14	41 ± 0.9	823	340	0.44 ± 0.1	4.8 ± 0.2
No PE	70:30 bPC:Chol	50:15:30:4:1 bPC:bPS:Chol:PI:PIP2	5	33.2 ± 3.4	340	113	0.47 ± 0.04	7.8 ± 1.1
PE Proximal	45:25:30 bPC:bPE:Chol	50:15:30:4:1 bPC:bPS:Chol:PI:PIP2	5	14.6 ± 1.7	419	58	0.38 ± 0.06	4.5 ± 1.0
PE Both	45:25:30 bPC:bPE:Chol	25:25:15:30:4:1 bPC:bPE:bPS:Chol:PI:PIP2	5	29.0 ± 3.1	455	134	0.38 ± 0.03	4.3 ± 0.5

Supplemental Table S1: *Summary of statistics of DCV fusion events with planar supported bilayers under different PE lipid conditions.* ***.*** *All events were fit with a parallel reaction model ($N(t) = N(1-e^{-kt})^m$ where N is the fusion probability, k is the rate, and m is the number of parallel reactions occurring, see ref. 19) for the cumulative distribution function of delay times between docking and fusion for single DCV events under different PE lipid conditions. Errors for k and m represent standard fitting errors obtained from a nonlinear Levenberg-Marquardt fit algorithm (34).*